

This article appeared in a journal published by Elsevier. The attached copy is furnished to the author for internal non-commercial research and education use, including for instruction at the authors institution and sharing with colleagues.

Other uses, including reproduction and distribution, or selling or licensing copies, or posting to personal, institutional or third party websites are prohibited.

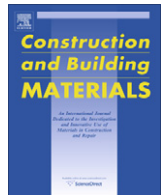
In most cases authors are permitted to post their version of the article (e.g. in Word or Tex form) to their personal website or institutional repository. Authors requiring further information regarding Elsevier's archiving and manuscript policies are encouraged to visit:

<http://www.elsevier.com/copyright>



Contents lists available at ScienceDirect

Construction and Building Materials

journal homepage: www.elsevier.com/locate/conbuildmat

Stereovision measurements on evaluating the modulus of elasticity of wood by compression tests parallel to the grain

J. Xavier^a, A.M.P. de Jesus^{b,*}, J.J.L. Morais^a, J.M.T. Pinto^a^a CITAB, University of Trás-os-Montes and Alto Douro, 5001-801 Vila Real, Portugal^b IDMEC-FEUP, University of Trás-os-Montes and Alto Douro, 5001-801 Vila Real, Portugal

ARTICLE INFO

Article history:

Received 4 January 2011

Received in revised form 29 April 2011

Accepted 13 June 2011

Available online 13 July 2011

Keywords:

Compression tests

Modulus of elasticity

Stereovision

Wood

ABSTRACT

In this work, the evaluation of the longitudinal modulus of elasticity (E_L) of maritime pine (*Pinus pinaster* Ait.) was investigated by means of compression tests parallel to the grain. Strain data was collected by digital image correlation (DIC) and compared with results from glued strain gauges. The DIC method provided similar results compared to the strain gauge measurements, but with reduced scatter due to higher gauge area, making the technique less sensitive to the wood heterogeneity (earlywood and latewood layers). The influence of the specimen parasitic end-effects (i.e., friction and damage) on the apparent modulus of elasticity was further investigated by testing specimens with different cross-sections and lengths. The apparent modulus of elasticity is underestimated for increasing specimen cross-sections and decreasing specimen lengths. Friction has a negligible effect on apparent modulus of elasticity, while the extension of the damaged contact zone is the governing phenomenon.

© 2011 Elsevier Ltd. All rights reserved.

1. Introduction

At the macroscopic scale (10–200 mm) clear wood (i.e., without knots, gross grain deviation or other structural features) is usually modelled as a homogeneous and continuous material. Moreover, the geometry and the arrangement of wood cells are locally defined by three orthogonal axes of material symmetry in longitudinal (L , 1), radial (R , 2) and tangential (T , 3) directions. Mechanical properties along these directions are usually determined by independent mechanical tests in which a uniform strain state is assumed across the gauge section. Therefore, due to the orthotropy and inherent variability of wood, a great effort is required for the material characterisation in terms of testing and equipment. To overcome some of these drawbacks, relationships have been proposed among different elastic properties [1] or relating elastic properties to density or moisture content of samples [2]. Within this framework, the modulus of elasticity of wood along the fibres (E_L) has been considered an independent variable, representing a fundamental wood property. Among other test methods (e.g., tensile or bending tests), this wood property can be determined by compression tests parallel to the grain. However, specimen parasitic end-effects can occur when carrying out this test, making difficult the data interpretation by conventional data reduction. These effects are usually understood to be associated to friction and damage occurring locally at the contact between the specimen and the compression plates.

Full-field optical methods of displacement or strain measurement have become very useful tools in experimental solid mechanics [3]. According to the physical phenomenon involved in the measurement, these methods can be classed into white-light techniques (e.g., digital image correlation and grid/moiré methods) and interferometric techniques (e.g., speckle and moiré interferometry and shearography). On the one hand, by comparison with conventional punctual techniques (e.g., strain gauges or extensometers), these methods have some important advantages: (i) they provide full-field data, and (ii) they are contact-free. On the other hand, full-field methods have a higher initial cost than conventional methods. Nevertheless, the use of optical methods in the analysis of wood deformation seems quite promising because of its inherent heterogeneity and anisotropy [4,5]. This work is intended to contribute to the application of full-field optical techniques in the framework of wood mechanics.

In this work, the compression test parallel to the grain for evaluating the longitudinal modulus of elasticity (E_L) of maritime pine (*Pinus pinaster* Ait.) was investigated by means of stereovision measurements. The influence of the aspect ratio of compression specimens on the correct evaluation of E_L was analysed by testing specimens with different cross-sections and lengths. For comparison purposes, the axial compressive strain state was measured by means of three different techniques. On the one hand, the stereovision (DIC-3D) optical technique was chosen for providing strain measurements. On the other hand, the strain state was determined by conventional techniques using both a linear strain gauge fixed at the centre of specimen, and the relative displacement between the compression plates measured by a linear variable differential

* Corresponding author. Tel.: +351 259 350 306; fax: +351 259 350 356.

E-mail address: ajesus@utad.pt (A.M.P. de Jesus).

transducer (LVDT). Note that no address is made in this work to other mechanical properties such as the Poisson's ratio or the compression proportional limit. Nevertheless, the full-field optical technique is a suitable method for simultaneous evaluation of several properties, since the strain state can be fully assessed during testing.

2. Compression test: data reduction

Let us consider the compression test method on a wood specimen oriented along the longitudinal direction (L , 1). According to the equilibrium and linear elastic constitutive equations, the following closed-form solution can be obtained for the identification of the longitudinal modulus of elasticity:

$$E_L = \frac{P}{A\epsilon_1} \quad (1)$$

where P is the applied compression load, A is the initial cross-section of the specimen and ϵ_1 is the linear strain along the longitudinal direction. Experimentally, the applied load (P) can be measured by the load cell of the testing machine. The axial compressive strain at the centre of specimen (ϵ_1) can be measured by different techniques. In this work, ϵ_1 was evaluated through: (1) the stereovision (DIC-3D) optical method, (2) a linear strain gauge glued at the centre and aligned with the longitudinal axis of the specimen, and (3) the relative displacement of the compression plates (contacting faces), with regard to the initial specimen length, measured by means of a LVDT. In the latter case, the machine stiffness is excluded due to the local measure of displacement provided by the LVDT.

3. Experimental work

3.1. Material and specimens

The wood samples tested in this work were cut from quarter-sawn and plain-sawn boards of a single *Pinus pinaster* tree (geographic origin: Portugal). These boards were previously dried in a kiln and then left in open air during several weeks. Specimens oriented along the grain were cut at the outermost part of these boards (mature wood) with different cross-sections $R \times T = 20 \times 20$, 30×30 and 40×40 mm² and lengths ($L = 30$, 60 and 120 mm) (Fig. 1), resulting nine test series. A total of 15 specimens per configuration were manufactured in a total of 135 specimens. The specimen dimensions of 20 (R) \times 20 (T) \times 60 (L) mm³ has been proposed in the ASTM D 143 standard [6] for determining the compression strength of wood along the longitudinal direction.

The temperature and the relative humidity of the laboratory were around 23 °C and 50%, respectively. The stabilisation of the specimens in laboratory was monitored by several successive weight measurements. The actual dimensions and weight of each specimen were also measured before testing and after stabilisation in the laboratory environment. The moisture content of specimens prior testing was about 10%, determined by the oven-dry method [7]. The oven-dry density of specimens (*i.e.*, the ratio between the oven-dry weight and the green volume) was in the range of 0.428–0.591 g/cm³.

3.2. Stereovision measurements

3.2.1. Choosing the method

The stereovision or 3D digital image correlation method (3D-DIC) was chosen in this work. This is a white-light technique and therefore more easily coupled with conventional apparatus – such as a universal testing machine – than an interferometric counter-

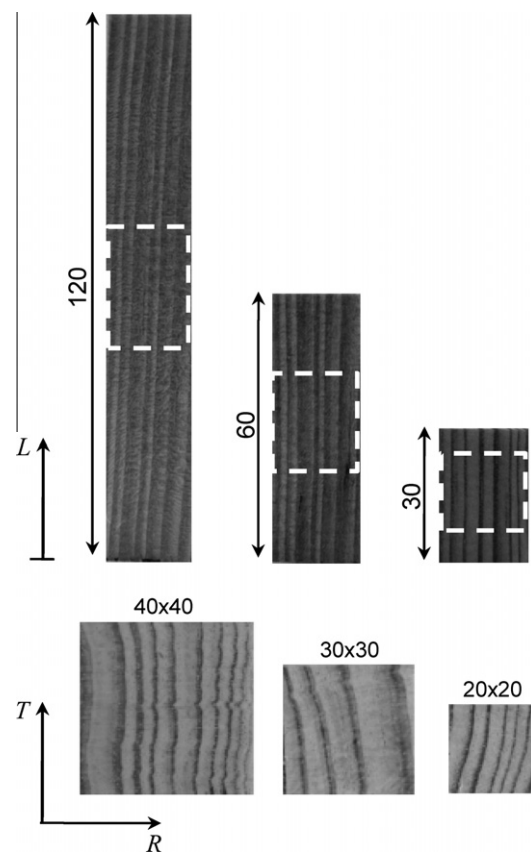


Fig. 1. Wood specimens tested in compression parallel to the grain (white dashed lines schematically represent the region of interest for digital image correlation, unit: mm).

part (namely because no specific equipment such as a laser or an anti-vibration table is required). Besides, considering the biological nature of the material, this technique has the advantage of being non-intrusive and requires simpler specimen preparation (speckle pattern) than other white-light techniques such as grid methods [4]. Moreover, the use of a stereovision system was advantageous in practice because: (i) there is more flexibility in terms of alignment and positioning of the optical system with regard to the specimen surface, and (ii) a measurement volume is defined through the calibration procedure of the stereovision system, so specimens can be tested sequentially afterwards, providing that they fit into this virtual space. However, when compared to a monovision system (DIC-2D), the main disadvantage is that the uncertainty on the evaluation of camera model parameters represents an additional uncertainty on the displacement measurement, and therefore on the evaluation of material properties.

3.2.2. Principle

Stereovision is a full-field optical technique for measuring the 3D (in-plane and out-of-plane) displacement/strain fields of a given 3D object. The analysis is based on pairs of stereo images recorded during the object deformation. A binocular stereovision (a measuring system with a pair of left and right cameras) is used for assessing the position of a 3D point in space (with regard to a given world coordinate system) from the knowledge of its stereo projection points in two recorded images (Fig. 2). This process is known as triangulation. On the one hand, this method requires a camera calibration consisting in determining the extrinsic (the relative position and orientation of the coordinates systems associated to the two cameras) and intrinsic parameters of the camera

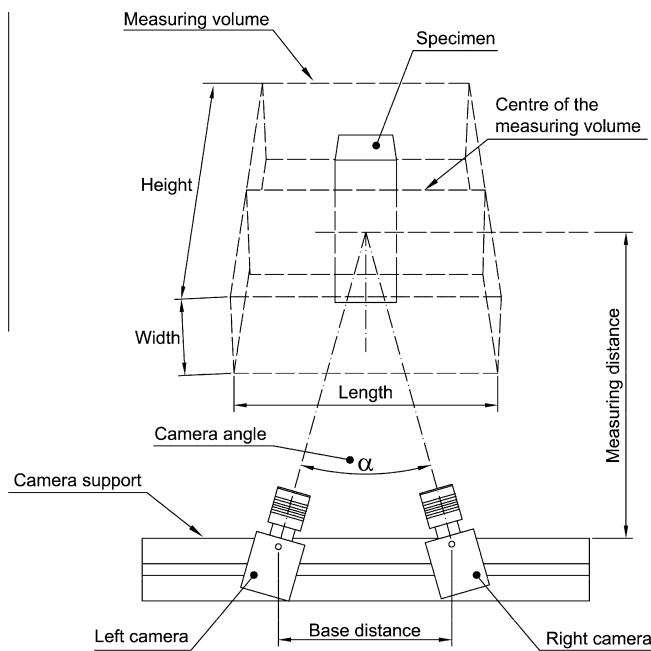


Fig. 2. Schematic representation of the stereovision measurement set-up (GOM-ARAMIS®).

model. On the other hand, a correspondence of the projection points on the two cameras must be established (stereo-matching problem) using for instance the epipolar constant concept. For a more complete description, a survey of the stereovision technique can be found in [8,9].

3.2.3. Photomechanical set-up and calibration

The GOM-ARAMIS® stereovision system was used in this work [10]. The optical system is equipped with two 8-bit Baumer® Optronic FWX20 cameras (resolution of 1624×1236 pixels, pixel size of $4.4 \mu\text{m}$ and sensor format of $1/1.8''$) coupled with two Schneider-Kreuznach® Componar-S 50 mm $f/2.8$ lenses (where f is the focal length of the lens). For mobility and adaptability, the cameras support was mounted on a Foba ALFAE tripod, which was positioned facing the testing machine (Fig. 3a).

The photo-mechanical set-up was adjusted as follows. Firstly, the optical system was positioned with regard to a specimen mounted into the mechanical set-up. A level ruler and a laser pointer were used to guarantee a correct alignment. Besides, the

specimen can be replaced by a mirror and the optical system set-up such that a laser beam illumination – throughout the direction of the bisecting line of the angle defined by the optical axes of the two cameras (Fig. 2) – would be perfectly perpendicular to the surface of the mirror. The measuring distance (defined between the specimen surface and the cameras support, Fig. 2) was set in the range of 300–500 mm, depending on the size of the region of interest of specimen to be tested (Fig. 1). The angle defined by the two cameras (α in Fig. 2) was chosen to be 25° . The base distance (defined between the rotating axes of the supports of the two cameras, Fig. 2) was adjusted in order to have coincidence between the centre of the specimen and the centre of the images recorded by the two (left and right) cameras. The two cameras were then focused, setting the lens aperture to $f/2.8$ to minimise the depth of field. The lenses aperture was then slightly closed ($f/11$) in order to improve the depth of field during calibration and testing. The shutter time was set to 100 ms, according to the cross-head displacement rate during testing (2 mm/min) and the size of the camera unit cells ($4.4 \mu\text{m}$). The light source was finally adjusted in order to guarantee an even illumination of specimen and to avoid over-exposition (i.e., the saturation of pixels above the dynamic range of the digital cameras).

The stereovision system must be calibrated before testing using a calibration object whose dimensions should be similar to that of the region of interest. Therefore, for the target regions of 20×20 , 30×30 and $40 \times 40 \text{ mm}^2$ (Fig. 1), the calibration panels of 15×12 , 25×20 and $35 \times 30 \text{ mm}^2$ were respectively used. In the first step, the calibration object was positioned into the mechanical set-up, with special attention to its coplanarity with regard to the geometrical plane that will be defined afterwards by the specimen surface (see Fig. 2). The calibration process is based on a set of images, taken successively by translating and rotating the calibration object with regard to the optical system. This leads to the definition of a measuring volume (Fig. 2), within which the specimens must be located during testing. After the alignment and the calibration of the optical system, the specimens can be mounted into the mechanical set-up and tested sequentially.

3.2.4. Surface preparation: speckle pattern

The digital image correlation method is based on the assumption that the object surface under analysis has a textured pattern such that the light intensity, diffusely reflected over the surface, will vary continuously with a suitable contrast. Different techniques have been successfully used for creation of such a speckle pattern, employing spray or airbrush paint, toner powder deposit or lithography [11]. In this work, the speckle pattern was created

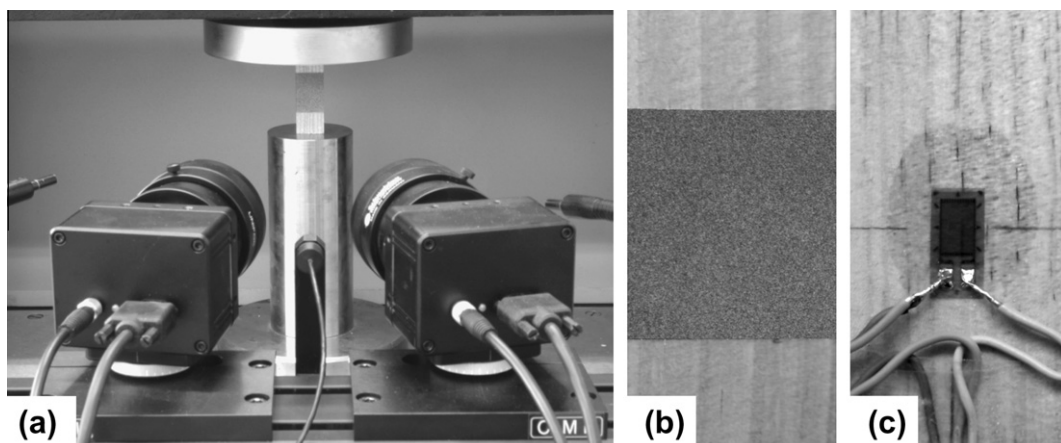


Fig. 3. Photomechanical set-up and specimen instrumentation: (a) stereovision set-up, (b) speckle pattern, and (c) strain gauge.

Table 1
Measuring parameters of GOM-ARAMIS® software.

<i>Project parameter – Facet</i>	
Facet size	15 × 15 pixels ²
Step size	15 × 15 pixels ²
<i>Project parameter – Strain</i>	
Computation size	3
Validity code	55%
Strain computation method	Total
<i>Stage parameter</i>	
Accuracy	0.04 pixels
Iteration limit	Enabled
Residual gray scale level	20 Gray levels
Intersection deviation	0.3
Acquisition frequency	0.2 Hz

by aerosol spray, applying a thin coating of white paint followed by a spot distribution of black paint (Fig. 3b).

3.2.5. Aramis measurement parameters

For the regions of interest of 20×20 , 30×30 and 40×40 mm² (Fig. 1), conversion factors of about 0.013, 0.020 and 0.027 mm/pixel were respectively defined (Table 1).

In the DIC method, the displacement field is measured by analysing the geometrical deformation of images of the surface of interest, recorded before and after deformation. For this purpose, the initial (undeformed) image is mapped by correlation windows (facets), within which an independent measurement of displacement is calculated. Therefore, the facet size on the object plane will define the spatial resolution of displacement. Typically, a large facet size will improve the precision of measurements but also will degrade the spatial resolution [12]. Thus, a compromise must be found according to the application to be handled. In this work, a fa-

cet size of 15×15 pixels was chosen, attending to the size of the region of interest, the optical system (magnification) and the quality of the granulate (average speckle size) obtained by the spray painting (Table 1). The facet step was also set to 15×15 pixels (Table 1), in order to avoid statistically correlated measurements.

The in-plane displacements were then numerically differentiated in order to determine the strain field needed for the material characterisation problem (Table 1).

3.2.6. Verification tests

3.2.6.1. Motionless tests. In order to estimate the measuring system accuracy, motionless tests were performed after calibration, consisting in recording several images of a target object without applying any deformation. These images were then processed based on digital image correlation, in order to compute the 3D full-field displacements. Noisy maps were typically obtained as shown in Fig. 4a (e.g., U_Y displacement field). The noisy displacement signal follows the trends of a Gaussian normal distribution, as it can be seen from the histogram plot (Fig. 4b). From this information the resolution of the method can be globally assessed on a statistical basis. The mean value over the whole field was used to quantify the systematic (bias) error of the method (Fig. 4c). Typically, values in the range of 0.15–0.32 μm were determined for the in-plane displacement (U_X and U_Y), whilst a value of about 0.50 μm was obtained for the out-of-plane displacement (U_Z). The standard deviation was taken as a measure of the method accuracy (Fig. 4d). For the U_X and U_Y displacements a value of about 0.16 μm was measured, whereas a value of 0.75 μm was found for U_Z .

3.2.6.2. Rigid-body translation tests. Rigid-body translation tests were also performed to assess the accuracy of the measuring system. A sample was mounted on a micrometer translation stage

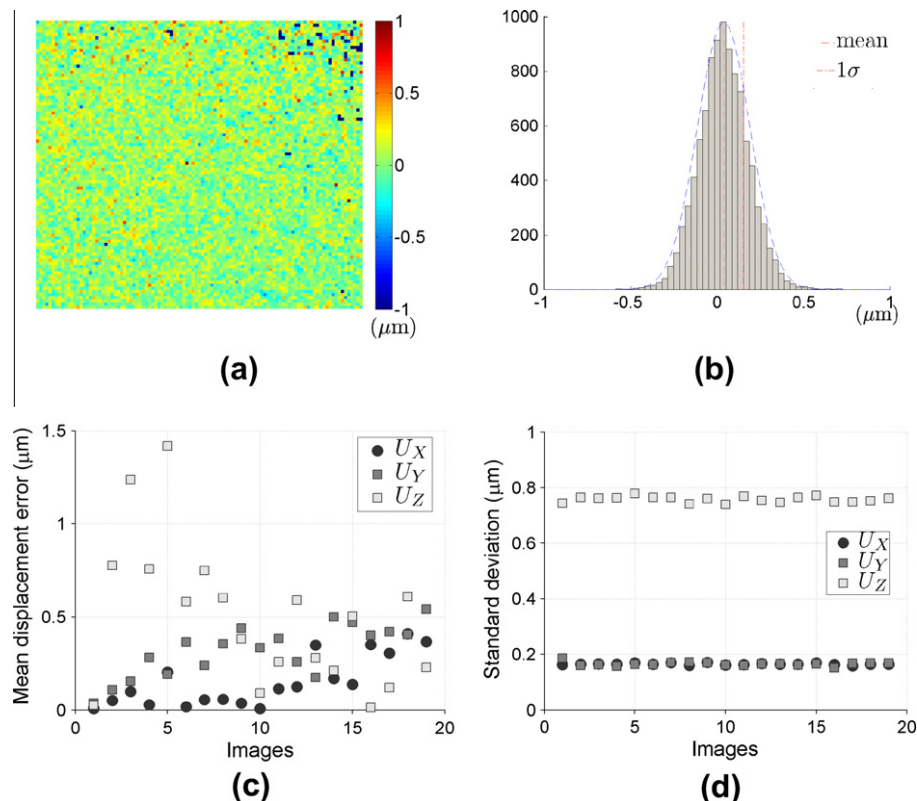


Fig. 4. Motionless tests: (a) U_Y noisy displacement field, (b) U_Y histogram plot, (c) mean (systematic) displacement error, and (d) standard deviation (accuracy).

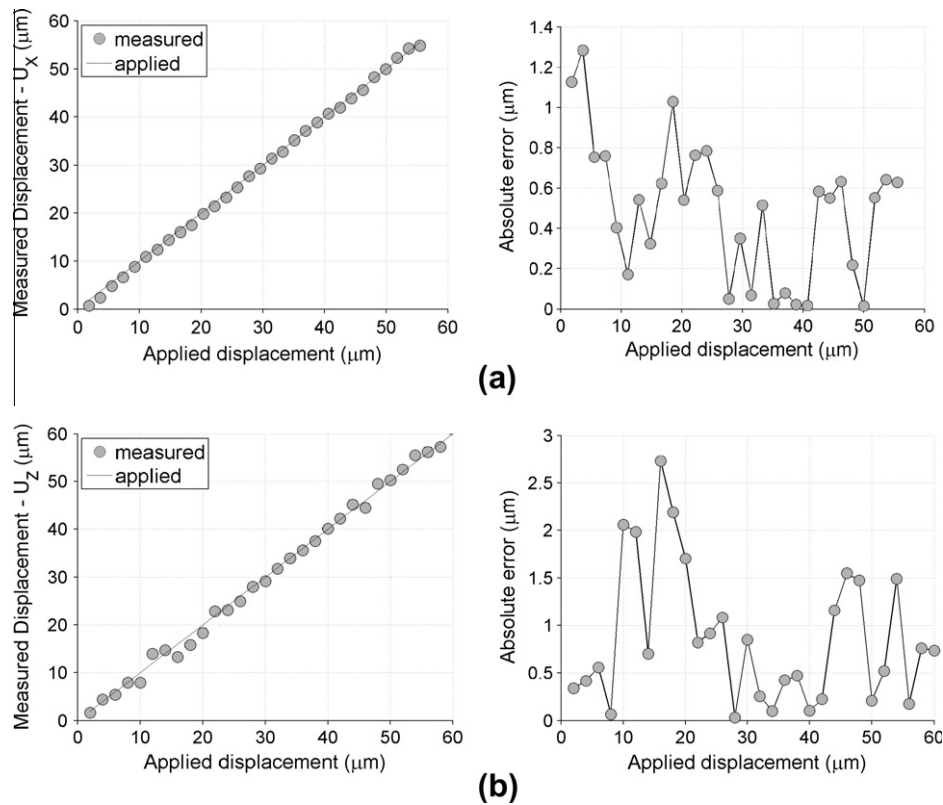


Fig. 5. Rigid-body translation tests: measured and absolute error of the: (a) U_x and (b) U_z displacements as a function of the applied displacement (step increment of 2 μm –0.02 pixels).

(resolution of 1 μm) and a sequence of images was recorded by applying successive displacement increments along the X (in-plane) and Z (out-of-plane) directions of 0.001 mm up to 0.030 mm. From the optical set-up a conversion factor of 0.017 mm/pixel was determined (a ruler imaged over the field of view was used for this calculation). This means that for each displacement increment there is a displacement of 0.056 pixels between successive images. At each stage, the average and standard deviation values over the whole calculated displacement field were evaluated (Fig. 5). As it can be seen, the calculated displacements are in relatively good agreement with the actual applied displacement, even though by computing the out-of-plane displacement some deviations were observed, which could eventually come from some bias by manually applying the displacement increments.

3.3. Compression tests parallel to the grain

The compression tests were carried out on an Instron 1125 universal testing machine under crosshead displacement control at a rate of 2.5 mm/min. The load was measured by a 100 kN load cell. Although the ASTM D 143 standard [6] recommends the use of spherical bearings in at least one plate of the testing machine, specimens were mounted between fixed plates in this work. All tests were instrumented for stereovision measurements. Images were grabbed during testing with a frequency of 0.2 Hz – the synchronisation with the load recording was achieved through a trigger box – (Table 1). Besides, the relative displacement of the compression plates was measured by means of a LVDT, model AML/EU \pm 10-S10 (displacement range of \pm 10 mm) from Applied Measurements®. Two specimens per configuration were also instrumented with strain gauges (Vishay Micro-Measurements, type EA-06-031DE-350 with a gauge grid of $3.05 \times 5.97 \text{ mm}^2$) glued at the back face of samples (see Fig. 3c). The M-Bond AE-

10® adhesive was used for the gauge fixing. The data (load, LVDT and strain measurements) were recorded by a HBM® SPIDER 8 acquisition system. Before testing, the specimens were loaded and unloaded five times up to a force of about 500 N, in order to accommodate the specimens into the plates.

4. Results and discussion

4.1. Evaluation of the modulus of elasticity

The evaluation of the modulus of elasticity by the compression test parallel to grain is presented and discussed with regard to the techniques used for measuring the strain. To start with, a

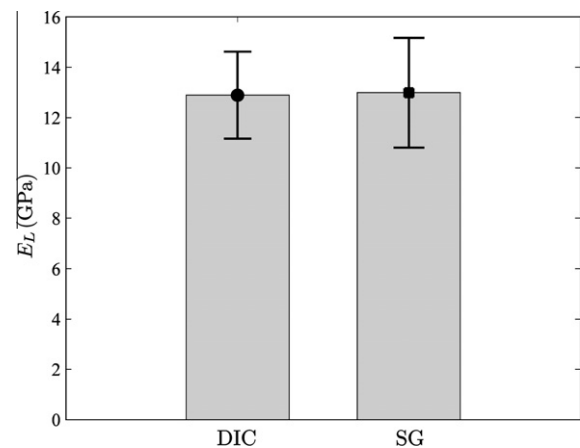


Fig. 6. Comparison of longitudinal modulus of elasticity determined from stereovision (DIC) and strain gauge (SG) measurements.

Table 2

Average values and standard deviations of the longitudinal modulus of elasticity obtained from stereovision measurements, for each test series (unit: GPa).

Cross-section (mm ²)	Height, <i>h</i> (mm)		
	30	60	120
20 × 20	15.7 ± 2.7	15.9 ± 3.1	14.5 ± 2.0
30 × 30	16.9 ± 2.9	15.1 ± 3.0	15.1 ± 2.9
40 × 40	18.1 ± 1.7	16.1 ± 2.7	15.8 ± 2.3

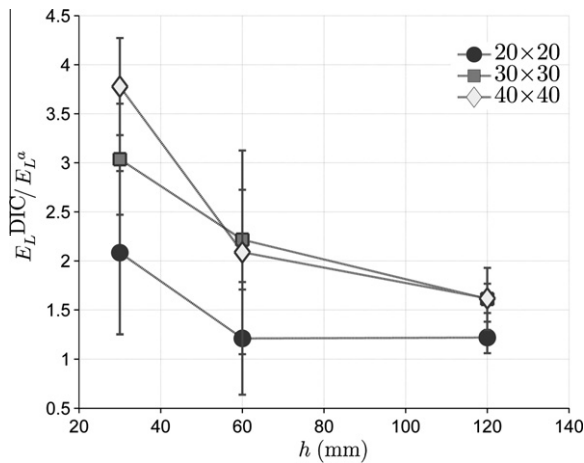


Fig. 7. Variation of the E_L^{DIC}/E_L^a ratio as a function of the geometry of the specimens (E_L^{DIC} is the modulus of elasticity determined from the stereovision measurements, whilst E_L^a is the apparent modulus of elasticity determined directly from load and relative displacement of the compression plates measured by LVDT).

comparison between stereovision and strain gauge measurements was carried out. Only data obtained for all specimens instrumented with both techniques were used in this analysis. Regarding the stereovision technique, the strain was evaluated by averaging the strains over the entire target region (Fig. 1). The summary of this study is presented in Fig. 6, in which the longitudinal modulus of elasticity determined from both stereovision and strain gauge measurements are compared. As it can be concluded, the same mean value of E_L is obtained from both measurement methods, according to the *t*-test for equality of means at the 95% confidence

level. Besides, a slightly higher scatter is observed for the strain gauge measurements than the stereovision ones. This result can be understood by the fact that the full-field measurements average the specimen deformation over a large area covering several annual growth rings, and therefore being less sensitive to the material heterogeneity at growth ring scale (earlywood and latewood layers) than the local strain gauge measurements. This result enhances the interest of full-field measurements when testing a heterogeneous material like wood.

Table 2 summarises the average and standard deviation values of the modulus of elasticity measured in the longitudinal direction, using the stereovision technique for each test series. These values are in close agreement with reference values for the *Pinus pinaster* Ait. species [13]. The modulus of elasticity from stereovision (E_L^{DIC}) was also compared with the apparent modulus of elasticity (E_L^a) computed directly from the applied load and the relative displacement of the machine plates given by LVDT measurements. This comparison is summarised in Fig. 7, where the ratio E_L^{DIC}/E_L^a is plotted as function of specimen length (*h*), for different cross-sections (20 × 20, 30 × 30 and 40 × 40 mm²). As expected, the apparent modulus of elasticity estimated from the LVDT measurements is systematically underestimated. Specimens with high lengths and small cross-sections seem to reduce this bias. Specifically, the cross-section of 20 × 20 mm² and specimen lengths higher than 60 mm yields more consistent values of the modulus of elasticity. It is worthwhile to note that the 20 × 20 × 60 mm³ specimen is recommended in the ASTM D 143 standard [6] for compression strength characterisation.

Fig. 7 shows large discrepancies on the modulus of elasticity values from specimens with short length and high cross-section. In order to point out this issue, friction effects and damage at the contact between the specimens and the loading plates are analysed in the following, based on an analytical/numerical point of view.

4.2. Friction effects on compression tests of prismatic specimens of clear wood

In order to assess the effects of friction between the end surfaces of the specimen and the loading plates on the compression test results, finite element models were used. These models were used to verify how friction influences the apparent modulus of elasticity. This influence was checked for several dimensions, namely, for several height/width ratios.

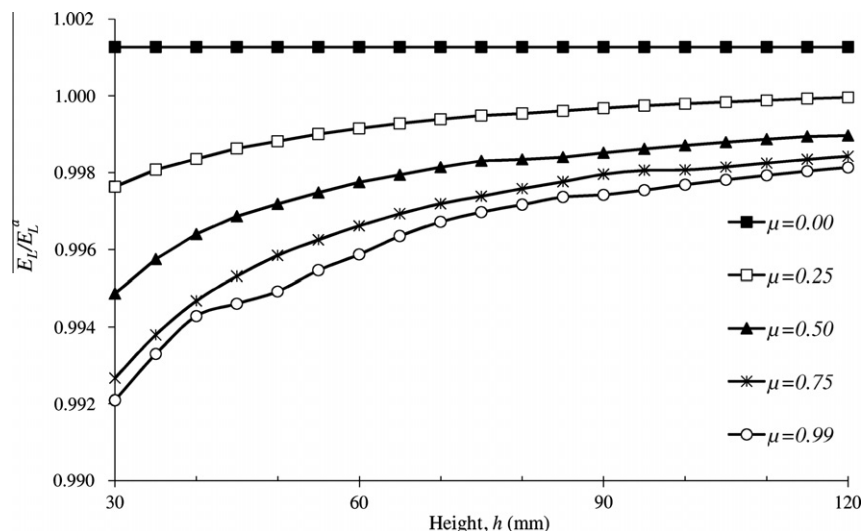


Fig. 8. Evolution of the apparent modulus of elasticity with the friction coefficient and specimen height (cross-section = 20 × 20 mm²).

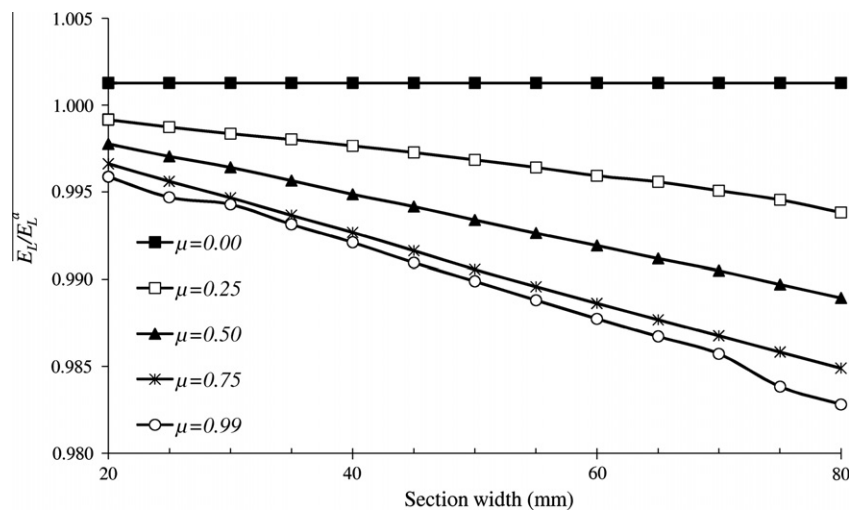


Fig. 9. Evolution of the apparent modulus of elasticity with the friction coefficient and specimen cross-section (height, $h = 60$ mm).

A parametric finite element model of the compression test was built using ANSYS® software. The wood specimen was modelled with 20-noded isoparametric solid finite elements. Two rigid-to-flexible contact surfaces were created to model the contact between the loading plates (target/rigid surfaces) and the faces of specimen (contact/flexible surfaces). The Augmented Lagrange contact algorithm was used together with the Coulomb friction model. The wood was modelled as an orthotropic and linear elastic material. The numeric penetration between the contact and target surfaces, which is inherent to the Augmented Lagrange contact algorithm, was kept at very low values.

The parametric finite element model was used to investigate the effect of friction on the apparent modulus of elasticity, taking into account several specimen dimensions, namely distinct specimen heights and cross-sections. Two series of simulations were carried out: (1) the first considered a fixed specimen width (20×20 mm²) and heights in the 30–120 mm range, and (2) the

second series considered a fixed height ($h = 60$ mm) and specimen cross-sections in the 20×20 mm²– 80×80 mm² range. Friction coefficient values in 0–0.99 range were tested for each geometry.

The evolution of apparent modulus of elasticity (E_L^a), normalized by the reference modulus of the elasticity (E_L) inputted in the finite element models, with respect to the friction coefficient and dimensions of specimens is shown in Figs. 8 and 9. The analysis of these figures reveals that frictionless results are not sensitive to the geometry effects. For this theoretical case, the apparent modulus should be equal to the modulus of elasticity. However, numerical results show an apparent modulus slightly higher than the modulus of elasticity, which is due to the residual numerical penetration of the rigid plate through the flexible contact surface. Therefore, curves shown in Figs. 8 and 9 should be corrected by a slight shift downward.

The numerical results show that friction is responsible for an apparent modulus higher than the true modulus of elasticity.

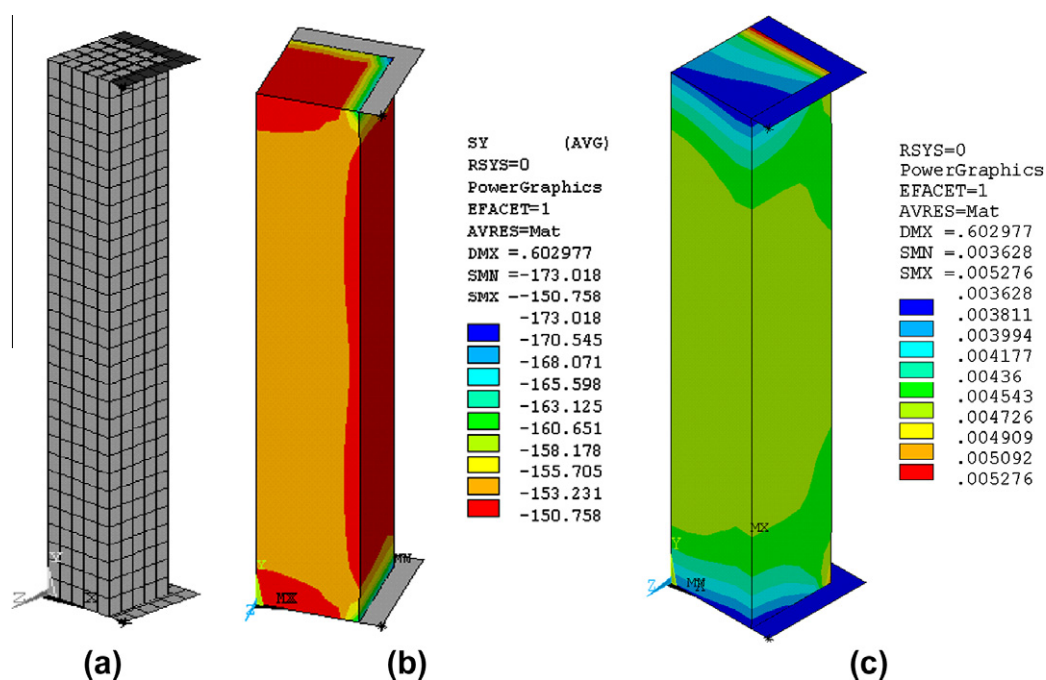


Fig. 10. Finite element model: (a) mesh of $1/4$ of the geometry, (b) longitudinal stress field (MPa), and (c) longitudinal strain field (specimen size = $20 \times 20 \times 60$ mm³).

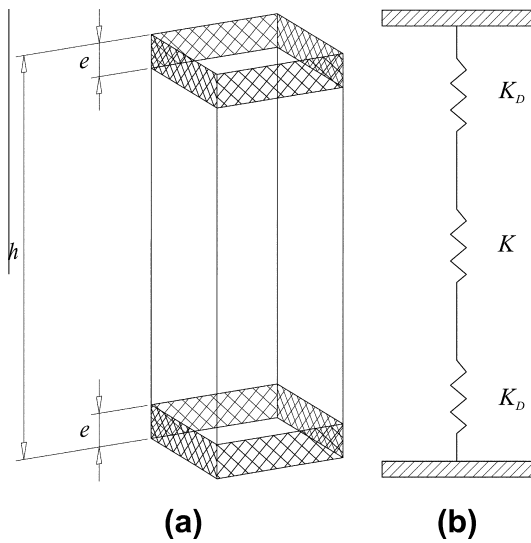


Fig. 11. Specimen with contact damaged zone: (a) geometry, and (b) spring model.

However, this effect fades with increasing height of the specimens and decreasing cross-section width, as illustrated by Figs. 8 and 9. Additionally, friction has only a marginal influence on the apparent modulus. This effect is contrary to the effect observed in experimental tests, where the apparent modulus is significantly lower than the true modulus. Therefore, the divergence between the apparent and true modulus of elasticity observed in the experimental results may not be justified by friction effects.

Friction induces a non-uniform longitudinal stress and strain field inducing a “barrel” deformation effect in the specimen, being responsible for the increasing apparent modulus. Fig. 10 shows the longitudinal stress and strain fields for a displacement of 0.01 times the height of the specimen, applied to the rigid plate, and a friction coefficient of 0.5.

4.3. Contact damaged zone effects on compression tests of prismatic specimens of clear wood

The experimental data results in an apparent modulus significantly lower than the modulus of elasticity (Fig. 7), which is not

justified by friction effects. The stiffness of the machine was excluded from the LVDT displacement measurements; therefore, it does not justify the lower apparent modulus. An explanation for this lower apparent modulus of elasticity is the existence of a contact damaged zone. This contact damaged zone may be justified by the cutting of the specimens which induces a local damage at the wood microstructure and also due to non-perfect contact (geometrical defects). A simple analytical spring model is proposed to investigate this phenomenon. The specimen is modelled as a series of three springs, as illustrated in Fig. 11. The stiffness of the virgin and damaged wood may be equated as follows:

$$K = \frac{E_L A}{h - 2e}, \quad (2)$$

$$K_D = \frac{E_L (1 - D) A}{e}, \quad (3)$$

where K is the stiffness of the virgin wood, K_D is the stiffness of the damaged material, E_L is the modulus of elasticity, h is the height of the specimen, e is the thickness of the damaged material, A is the cross-section of the specimen and D is the damage.

The equivalent stiffness of the specimen (K_{eq}) is expressed as follows:

$$K_{eq} = \frac{1}{\frac{2}{K_D} + \frac{1}{K}} = \frac{E_L A}{(h - 2e) + \frac{2e}{(1-D)}}. \quad (4)$$

The apparent modulus of elasticity (E_L^a) is finally calculated using the following equation:

$$E_L^a = K_{eq} \frac{h}{A} = \frac{E_L h}{(h - 2e) + \frac{2e}{(1-D)}}. \quad (5)$$

Fig. 12 illustrates the influence of the damage (D) and thickness of the damaged material (e) on the apparent modulus of elasticity. The results are shown for a reference specimen of $20 \times 20 \times 60 \text{ mm}^3$. This damaged material explains an apparent modulus of elasticity lower than the true one. The experimental results of Fig. 7 show, for specimens with $20 \times 20 \times 60 \text{ mm}^3$, an average E_L/E_L^a ratio of about 1.25. This experimental result is consistent with a damaged material of $e = 5 \text{ mm}$ and a damage $D = 0.6$.

Fig. 13 shows the evolution of the apparent modulus of elasticity with the specimen height and damage level of the damaged contact zone of specimen. The thickness of the damaged material was kept equal to 5 mm. The figure shows that the material

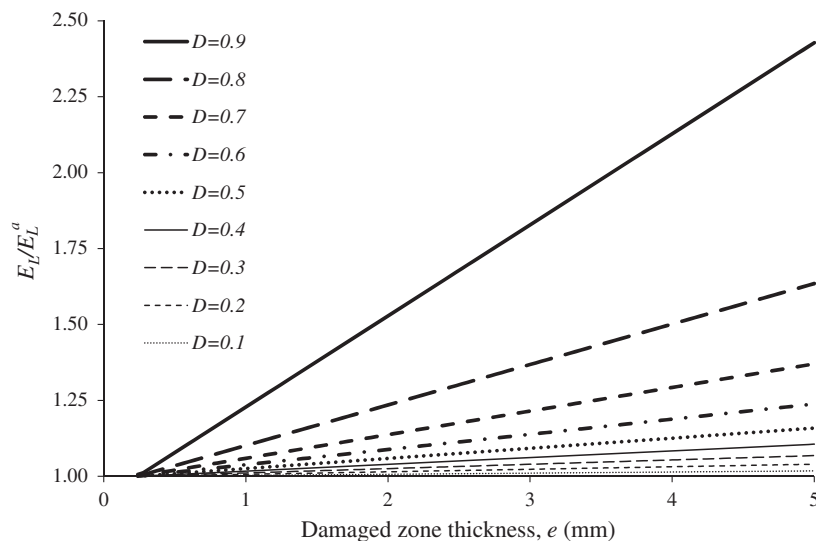


Fig. 12. Effect of damage and damaged zone thickness on apparent modulus of elasticity (specimens of $20 \times 20 \times 60 \text{ mm}^3$).

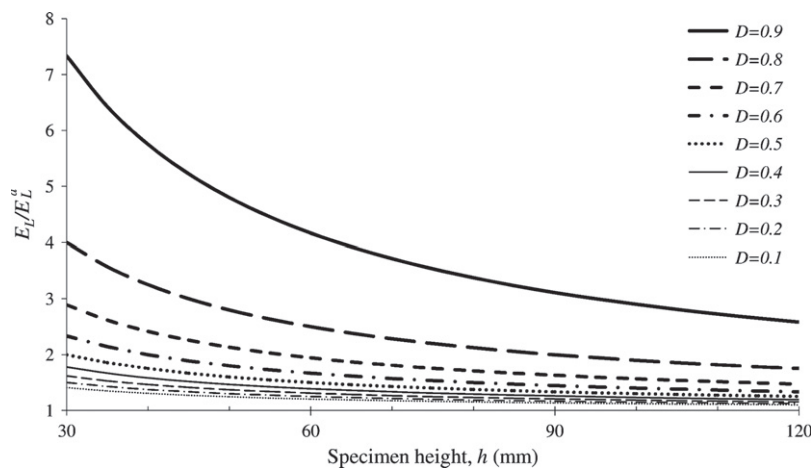


Fig. 13. Effect of damage and specimen height on apparent modulus of elasticity (section of $20 \times 20 \text{ mm}^2$; damage zone thickness, $e = 5 \text{ mm}$).

apparent modulus reduces with the increasing of specimen height. Considering a specimen of $20 \times 20 \times 30 \text{ mm}^3$ with damage equal to 0.6, a E_L/E_L^a ratio of about 2.4 is found. The experimental result shown in Fig. 7 is about 2.1, which is the same order of magnitude. The experimental results illustrated in Fig. 7 shows that both height and cross-section of specimens influences the apparent modulus. The influence of height is accounted for explicitly in Eq. (5). The cross-section does not appears explicitly in Eq. (5), but the cross-section should influence the apparent modulus of elasticity through the damage level, D , and the damaged zone size, e .

5. Conclusions

This work addresses the evaluation of longitudinal modulus of elasticity (E_L) of maritime pine (*Pinus pinaster* Ait.) by compression tests parallel to grain. The application of the stereovision method for determining the axial compressive strain was found advantageous, since an average value could be calculated on a base distance covering several annual growth rings and thus being less sensitive to the material heterogeneity. Hence, the stereovision method led to less scatter in the identification of the modulus of elasticity than strain gauge measurements.

The influence of parasitic end-effect, occurring locally nearby the contact between the specimen and the compression plates, on the apparent modulus of elasticity was investigated by testing wood samples with different aspect ratios. The discrepancy between the apparent and representative modulus of elasticity, obtained using DIC-3D, may be attributed mainly to a contact damage zone, since friction had a negligible and opposing effect, as shown by finite element analysis. The proposed analytical model shows that a damage zone with an order of magnitude of 5 mm and damage level of 0.6 should give consistent results for the

reference specimen geometry of $20 \times 20 \times 60 \text{ mm}^3$. However, the analytical model is not able to explain the section size effects experimentally observed.

References

- [1] Bodig J, Goodman R. Prediction of elastic parameters for wood. *Wood Sci* 1973;5(4):249–64.
- [2] Smith I, Landis E, Gong M. *Fracture and fatigue in wood*. John Wiley and Sons; 2003.
- [3] Grédiac M. The use of full-field measurement methods in composite material characterization: Interest and limitations. *Compos Part A – Appl Sci* 2004;35(7/8):751–61.
- [4] Xavier J, Avril S, Pierron F, Morais J. Novel experimental approach for longitudinal-radial stiffness characterisation of clear wood by a single test. *Holzforschung* 2007;61(5):573–81.
- [5] Dahl KB, Malo KA. Planar strain measurements on wood specimens. *Exp Mech* 2009;49(3):575–86.
- [6] ASTM. Standard methods of testing small clear specimens of timber (D143–94). Annual book of standards, vol. 04.10. Philadelphia (PA), USA: American Society for Testing and Materials; 2000.
- [7] ASTM. Standard test methods for direct moisture content measurement of wood and wood-base materials (D4442–92). Annual book of standards, vol. 04.10. Philadelphia (PA), USA: American Society for Testing and Materials; 1997.
- [8] Orteu J-J. 3-D computer vision in experimental mechanics. *Opt Laser Eng* 2007;47(3/4):282–91.
- [9] Sutton M, Orteu J-J, Schreier H. *Image correlation for shape, motion and deformation measurements: basic concepts, theory and applications*. Springer; 2009.
- [10] GOM mbH. ARAMIS commercial software. Aramis 6.0.2; 2000.
- [11] Sutton MA, McNeill SR, Helm JD, Chao YJ. Advances in two-dimensional and three-dimensional computer vision. In: Rastogi PK, editor. *Photomechanics – topics in applied physics*. Verlag: Springer; 1999.
- [12] Lecompte D, Smits A, Bossuyt S, Sol H, Vantomme J, Van Hemelrijck D, et al. Quality assessment of speckle patterns for digital image correlation. *Opt Laser Eng* 2006;44(11):1132–45.
- [13] Xavier JC, Garrido NM, Oliveira M, Morais JL, Camanho PP, Pierron F. A comparison between the Iosipescu and off-axis shear test methods for the characterization of *Pinus pinaster* Ait. *Compos Part A – Appl Sci* 2004;35(7–8):827–40.